Macromolecules

pubs.acs.org/Macromolecules Article

Water Domain Enabled Transport in Polymer Electrolytes for Lithium-Ion Batteries

Matthew D. Widstrom, Oleg Borodin, Kyle B. Ludwig, Jesse E. Matthews, Sahana Bhattacharyya, Mounesha Garaga, Arthur V. Cresce, Angelique Jarry, Metecan Erdi, Chunsheng Wang, Steven Greenbaum, and Peter Kofinas*

Cite This: *Macromolecules* 2021, 54, 2882–2891 Read Online

ACCESS | Metrics & More | Article Recommendations | Supporting Information

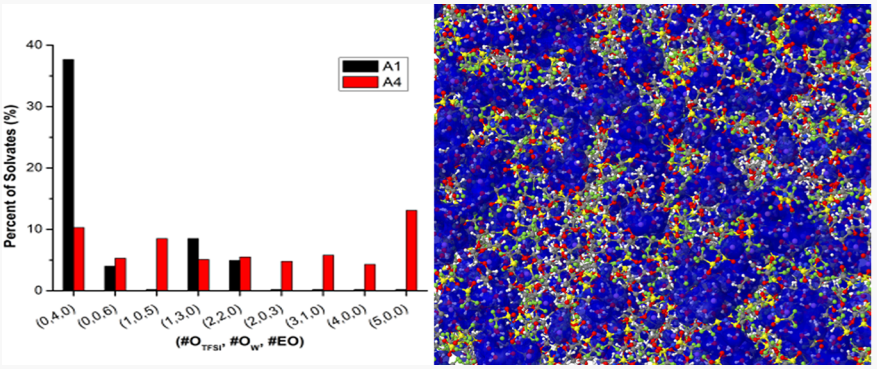

ABSTRACT: Widespread commercial adoption of polymer electrolytes for lithium-ion batteries has been hindered by subpar transport properties, namely, ionic conductivities of <1 mS/cm at room temperature and slower Li^+ compared to anion transport. The developed polymer and water-in-salt electrolyte demonstrated preferential Li^+ transport compared to the anion via pulsed field gradient NMR, acceptable ionic conductivities of >1 mS/cm at 25 °C, and an extended electrochemical stability window compared to water-in-salt electrolytes. This polymer electrolyte has a flexible liquid/solid transition through polymer molecular weight tuning, and both liquid and solid iterations are investigated. MD simulations provided additional insight into the Li^+ solvation environment and the mechanism of fast, preferential Li^+ transport through percolation of water-rich $Li^+(H_2O)_n$ nanodomains inside the poly(ethylene oxide) matrix.

INTRODUCTION

Current state-of-the-art lithium-ion batteries (LIBs) rely on liquid organic electrolytes to create passivating interfaces to enable high voltage battery configurations (>4.0 V). Electrolyte solvents such as ethylene carbonate (EC) and dimethyl carbonate (DMC) provide sufficient ionic conductivity and stabilize the electrolyte−graphite interface by decomposing and forming an electronically insulating but ionically conducting solid electrolyte interphase (SEI). However, these solvents are inherently flammable and are often coupled with a thermally unstable salt ($LiPF_6$).[1] The choice of thermally unstable components for the sake of performance makes the battery susceptible to multiple failure modes that would result in thermal runaway and combustion, generating significant interest in replacing these liquid electrolytes with safer materials.[2−6] Solid electrolytes are attractive alternatives to liquid organic electrolytes from a safety perspective as they could address many of the failure modes such as electrolyte leakage, high temperatures, overcharging, and fire.[1] Liquid organic electrolytes exhibit an intense exothermic reaction above 200 °C,[7] and PEO + salt "dry SPEs" are more thermally stable. However, these SPEs have also been shown to burn in a flammability test,[8] proving that thermal stability and safety are still a concern with these dry SPEs. Another major limitation hindering dry SPE adoption is their poor ionic conductivities (<10^{-4} S/cm).[9−13] Attempts to improve conductivity often focus on plasticizing the polymer matrix with the addition of various materials.[4,14−19] A more promising route, however, would involve decoupling ion motion from the structural relaxation and segmental motion of polymer chains.[20]

Angell et al.[21] first demonstrated in 1993 the concept of polymer-in-salt electrolytes (PiSEs), as opposed to the commonly studied salt-in-polymer electrolytes. With the

Received: August 25, 2020
Revised: February 14, 2021
Published: March 1, 2021

https://dx.doi.org/10.1021/acs.macromol.0c01960
Macromolecules 2021, 54, 2882–2891

Table 1. Compositional and Transport Properties of ASPEs Determined by Electrochemical Impedance Spectroscopy (EIS) and Pulsed Field Gradient Nuclear Magnetic Resonance (pfg-NMR)

sample	PEO content [wt %]	LiTFSI content [wt %]	water content [wt %]	Li/water mole ratio	Li^+/EO/water mole ratio	Li transport no. $[D(Li)/(D(Li) + D(F))]$ (unitless)[a]	EIS σ @ 25 °C [mS/cm][b]	Nernst−Einstein equation calculated σ @ 23 °C [mS/cm][c]
ASPE1	22.7	64.7	12.6	1:3.09	0.44:1:1.36	0.64	1.75 ± 0.132	3.67
ASPE2	23.1	66.0	10.9	1:2.64	0.44:1:1.16	0.67	1.58 ± 0.235	2.54
ASPE3	23.5	67.3	9.2	1:2.18	0.44:1:0.96	0.67	0.909 ± 0.123	1.76
ASPE4	24.0	68.5	7.6	1:1.73	0.44:1:0.76	0.66	0.681 ± 0.146	0.998

[a]Transport numbers are obtained from NMR experiments for various molecular species in the ASPEs at 25 °C. [b]Ionic conductivity is measured by EIS at 25 °C. [c]Conductivity is calculated using the Nernst−Einstein equation at 23 °C.

understanding that polymers such as poly(ethylene oxide) (PEO) or poly(propylene oxide) (PPO) show complete miscibility with many lithium salts, the relative concentration of salt and polymer could be inverted such that salt was the majority component. It was observed that in these salt-in-polymer systems, the glass-transition temperature (T_g), the temperature above which meaningful polymer segmental motion is experimentally observed, showed a maximum as salt content was increased, indicating that transport properties of the salt−polymer electrolyte could be improved by increasing the salt content past this maximum. This insight deviated from the conventional wisdom that as salt concentration increases, T_g increases.[22,23] The compositional range past the T_g maximum was named the salt-in-polymer domain, and it was demonstrated that as little as 10−20 wt % high-molecular-weight polyether (>10^5 Da) is needed to impart the mechanical properties of an elastomeric solid. Conductivity values greater than 10^{-4} S/cm at 25 °C were measured for 90% lithium salts and either 10% PEO or 10% PPO.[21] Bushkova et al.[24] described the transport properties in terms of percolation theory, with a critical threshold of ion clusters creating a network effect, effectively creating one big cluster. This allows for fast cationic transport of Li^+ through this cluster network by decoupling ion motion from polymer chain segmental motion, with this decoupling termed "superionic".[20] The attractive features of the PiSE approach are the combination of fast cationic transport with the mechanical properties of a flexible polymer. Ferry et al. showed that the role of the polymer, in addition to forming a solid, is to plasticize the salt and impart the ability to form an ion cluster network.[25]

Taking the concept of salt-rich systems, Suo et al.[6] innovated a highly concentrated 21 m (molal) solution of lithium bis(trifluoromethanesulfonyl)imide (LiTFSI) in water or "water-in-salt" electrolyte (WiSE). This is analogous to the PiSE, with the difference being that water is acting as the plasticizing agent as opposed to the high-molecular-weight polymer. However, similar to the PiSE, the WiSE is constructed to solve a fundamentally different problem than decoupling ion motion from chain segmental motion in polymer electrolytes. This system demonstrated for the first time that through superconcentration of lithium salts, anion reduction could be an effective route to the formation of a passivating SEI[6,26−29] in an aqueous electrolyte. Their research showed an expanded electrochemical stability window (ESW) for an aqueous electrolyte up to ∼3 V, with the proof of concept battery pair of a Mo_6S_8 anode and a lithium manganese oxide (LMO) cathode. This work has sparked interest in high salt concentration electrolytes for aqueous systems as a compositional approach to changing the mechanism for SEI formation, leading to further improvements through the use of additional salts[29−31] and hybrid aqueous/nonaqueous[32] systems. Switching from organic solvent to anion-derived passivation enabled by a high concentration of lithium salt (>3 M) constitutes a paradigm shift in interphase formation and opens a range of possibilities for tailoring the SEI that were previously unavailable, enabling higher voltage aqueous battery chemistries.

Building on the previous observation that in PiSE systems, residual amounts of solvent could improve the conductivity by multiple orders of magnitude,[33] we designed a polymer electrolyte composed of a polymer matrix doped with salt and plasticized with water that simultaneously improves polymer electrolyte safety and lithium cation transport. This polymer and water-in-salt electrolyte (pWiSE) also has improved electrochemical stability compared to the traditional WiSE. The inclusion of water can provide an extinguishing effect that significantly improves safety, which is a notable enhancement over dry SPEs.[8] Unlike previous study of a very low-molecular-weight oligomer of poly(ethylene glycol) (MW = 400),[34] we investigated incorporation of the WiSE into both a liquid/solid PEO polymer matrix to form an aqueous polymer electrolyte. Tuning the molecular weight of the polymer results in either an SPE or a liquid polymer electrolyte with the same chemistry, with the low-molecular-weight liquid variant allowing for easier electrochemical characterization with three-electrode cyclic voltammetry. Both variations of electrolytes demonstrate room-temperature conductivities of >1 mS/cm and exceptional cationic transport properties with $D(Li) > D(F)$. MD simulations reveal Li^+ solvating environments and the mechanism for high Li^+ conduction in these electrolytes with a focus on the vehicular motion of Li^+ as $Li^+(H_2O)_4$ versus solvent and anion exchange.

RESULTS AND DISCUSSION

Aqueous solid polymer electrolytes (ASPEs) were produced using a high-molecular-weight PEO matrix (10^6 M_v) to make free-standing polymer electrolyte membranes (the manufacturing process is depicted in Figure S1). The compositions of ASPE1−ASPE4 were designed by fixing the molar ratio of Li^+/EO (EO being total ethylene oxide repeat units in the system) to 1:0.44 while adjusting the molar component of water from 1.36 to 0.76 in 0.2 decrements. This was done to study the effect of water concentration on electrolyte properties. ASPE composition information in both weight percentages and relative molar concentrations can be found in Table 1. Low-molecular-weight aqueous polymer electrolyte solutions (designated AE1 and AE4) are made with the same molar ratios of ASPEs found in Table 1. However, the low-molecular-weight PEG (3350 M_n) forms a polymer solution as opposed to a solid membrane. AE1 and AE4 are referenced in the MD

https://dx.doi.org/10.1021/acs.macromol.0c01960
Macromolecules 2021, 54, 2882−2891

simulations as they are closer in molecular weight to what was modeled (PEO with 64 repeat units, molecular weight ≈ 2816 Da).

Differential scanning calorimetry (DSC) was used to identify the presence of any reversible phase transitions of ASPEs and to ensure that the relative concentrations of lithium salt and water were sufficient to fully plasticize the high-molecular-weight polymer matrix. Figure S2 shows DSC thermograms, measured at a temperature range of −40 to 100 °C for both the pure 1 M MW PEO matrix and for the ASPE2 composition that is representative of all ASPE compositions measured in the same temperature range. The polymer matrix exhibits a melting peak at ∼67 °C, which is consistent with literature values of a high-molecular-weight PEO melting transition.[35] The representative ASPE thermogram shows no melting or recrystallization peaks, confirming that the PEO component in the ASPE mixture is fully amorphous, which is the preferred morphology for ion conduction. The classic conduction model for PEO electrolytes is the forming and breaking of coordination bonds between EO and Li^+ in the amorphous fraction of the polymer where chains can be mobile.[36] It is well understood in the ethylene oxide-containing polymer−ion transport literature that there is a maximum in electrolyte ionic conductivity as a function of relative salt molar concentration (Li^+/EO).[37,38] Consequentially, there is a trade-off between increasing charge carriers and increasing T_g through higher salt content as a result of associations between the polymer and salt.[38−40] This maximum in ionic conductivity is often found to be at a lower salt concentration (Li^+/EO = 0.08 for LiTFSI in PEO)[38] and is the driving motivation for characterizing the T_g values of these ASPEs that have a relatively high Li^+/EO = 0.44. One could expect to see lower T_g values as water content, which has a strong plasticizer, is increased. To measure the T_g values of ASPEs, the temperature range was adjusted to scan colder than −40 °C, and the T_g value was taken as the onset temperature at which the slope of the thermogram changes. DSC scans for all ASPE compositions from −100 to 20 °C are shown in Figure 1. All ASPE compositions show a T_g value between −82 and −86 °C, indicated by red arrows. The fact that the T_g value for the ASPE system is approximately −85 °C

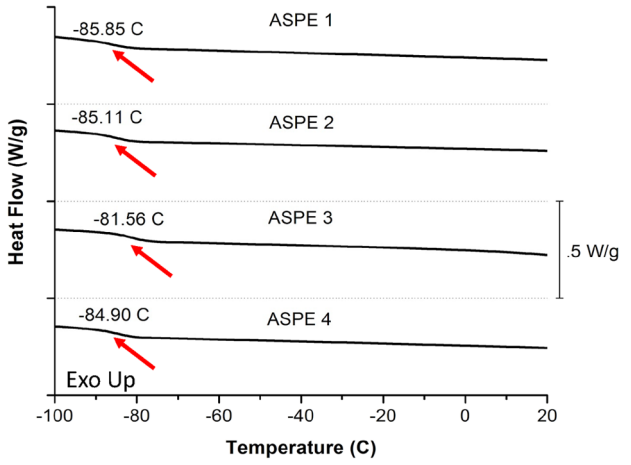

Figure 1. DSC thermograms of ASPE1−ASPE4 depicted on the same plot with a vertical offset of 0.5 W/g. All ASPE compositions show a T_g value in the temperature range of −82 to −86 °C. Glass-transition temperatures are indicated by each plot with a red arrow and temperature value.

shows the tremendous impact that water has as a plasticizer in this system. For context, PEO + LiTFSI salt mixtures with a Li^+/EO mole ratio of 0.44, the ratio used for ASPE1−ASPE4, exhibit a T_g value of 15 °C,[40] and high-molecular-weight PEO with no salt exhibits a T_g value of −67 °C.[41] It is evident that the inclusion of water in the electrolyte suppresses crystallinity and decreases T_g past what is observed for neat PEO, even in the presence of high lithium salt content. It is unclear how much water is needed to have this plasticization effect as the T_g values for ASPE1−ASPE4 are not appreciably different as the molar component of water changes from 1.36 to 0.76 in 0.2 decrements. Despite their amorphous nature, ASPEs behave mechanically as elastomeric solids with no wetness or leakage, shown in Figure S3 with a stress−strain relationship measured in tension and a picture of a stretched ASPE membrane.

The benefit of ASPE1−ASPE4 being amorphous is clearly seen in the ionic conductivities of the electrolytes. The room-temperature conductivity values for ASPE1−ASPE4, as measured by electrochemical impedance spectroscopy (EIS), are shown in Table 1 and are on the order of 10^{-3} S/cm. Conductivity values for ASPE1 and ASPE4 are plotted as a function of inverse temperature (over the range of 0 to 80 °C) in Figure 2A. The compositions show a clear trend of increasing conductivity with increasing water content, with ASPE1 and ASPE4 compositions being notably conductive for SPEs compared to their liquid analogues, tracking the conductivity of AE1 and AE4. In the case of ASPE4/AE4, the improved ionic conductivity of the solid variant is likely an artifact from water absorption during sample fabrication and transfer, leading to larger conductivity.[33] Thus, we consider the actual conductivity to be lower, with the values reported in Figure 2A for ASPE1 and ASPE4, establishing an upper bound. The lack of phase transitions evident in Figure S2 shows that the polymer matrix is fully amorphous due to plasticization by LiTFSI and water in the full compositional range investigated here. The conduction mechanism of PEO transport of Li^+ commonly results in electrolytes with conductivity values on the order of 10^{-6} S/cm in a semicrystalline system and values on the order of 10^{-4} S/cm in a fully amorphous system at elevated temperature past the melting point of the polymer matrix (∼67 °C). Fast ion transport in SPEs is a characteristic of the amorphous phase and is attributed to the inhibition of crystallization in the polymer matrix. Considering that the conductivity values of the ASPE system are a full order of magnitude higher than those of typical amorphous PEO electrolytes that have been plasticized with ionic additives at higher temperatures, it is likely that water plays an important role in the Li^+ transport mechanism. The disproportionation of Li^+ solvation into water-rich and anion-rich domains has been shown to occur in WiSE systems[42] and leads to $Li^+(H_2O)_n$ vehicular motion through $Li^+(H_2O)_n$ domains. The suggested dominant conduction mechanism of the pWiSEs investigated here is water-assisted vehicular transport, which is bolstered by the water concentration dependence of the conductivity results. The Li^+ solvation environment is further discussed in the MD simulation section below.

To further elucidate the transport properties of this ASPE system, NMR measurements were taken. Diffusion coefficients for fluorine (salt anion) and lithium (salt cation) are shown in Figure 2B as a function of temperature for ASPE1 and ASPE4. This data set was collected from samples that were prepared in an ambient atmosphere using a method for packing NMR tubes that involved rolling samples in parafilm. This

https://dx.doi.org/10.1021/acs.macromol.0c01960
Macromolecules 2021, 54, 2882−2891

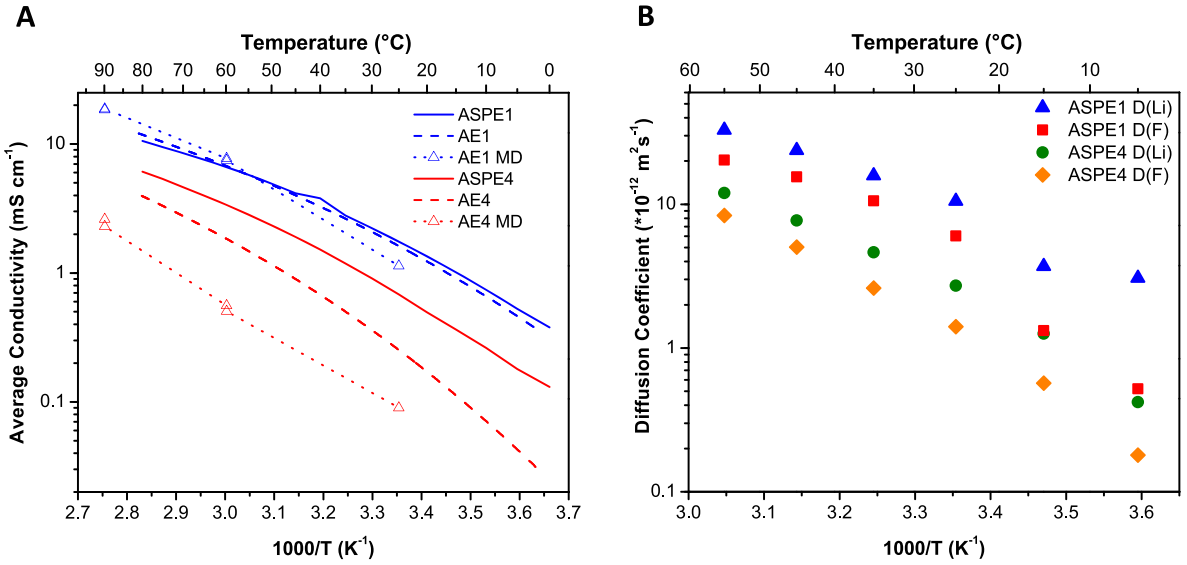

Figure 2. (A) Conductivity of solid and liquid pWiSE hybrid electrolytes from MD simulations and experiments. (B) pfg-NMR measured diffusion coefficients for the cation and anion in solid ASPE1 and ASPE4 expressed as a function of temperature. ASPE1 corresponds to the lowest value of Li/water, while ASPE4 corresponds to the highest value.

preparation method is illustrated in Figure S4 and resulted in preparation times of less than 5 min. These samples could not be used to measure proton diffusion (water) as there was too much background signal from parafilm. Numerical values for Li^+ and $TFSI^-$ diffusion coefficients are shown in Tables S1 and S2, respectively. A second sample set was prepared without parafilm packing so that proton diffusion coefficients could be measured. However, these samples took longer to prepare (~20 min) and likely absorbed ambient water during preparation (Figure S5). This difference in sample exposure to an ambient atmosphere made a difference in the results collected as the set of samples that was exposed to the atmosphere for longer time demonstrated higher diffusion coefficients for each species measured, likely due to water absorption. The other sample set (Figure 2B) has the added benefit of diffusion measurements for a range of temperatures while also being closer to intended sample compositions with less atmosphere exposure time.

The diffusion coefficients in Figure 2B are consequential on several counts. First, the room-temperature diffusion coefficients are an order of magnitude higher than those typically observed in more dilute (but water-free) PEO–salt complexes at temperatures above the melting point of PEO (~60 °C).[39] This is consistent with the high values of ionic conductivity from Figure 2A. Second, the cation diffusion coefficient exceeds that of the anion, which is counter to "classical" salt-in-polymer PEO complexes and to many PEO/salt/plasticizer systems.[41,43] In the latter case, the polyether segments preferentially solvate the cations. This leads to anions being largely unhindered by coordinating species, resulting in higher diffusion coefficients relative to Li^+, and hence cation transference numbers of ~0.2 to 0.3.[37] From the NMR measurements, it is possible to obtain a related cation transport number via eq 1

$$t^+ = \frac{D_+}{D_+ + D_-} \tag{1}$$

Those values calculated from the first NMR data set are listed in Table 1. It is important to note that the transport number is a less meaningful quantity than the electrochemical transference number in the presence of significant ion pairing. Additionally, the ionic conductivity can also be calculated using the diffusion coefficients measured by NMR via the Nernst–Einstein equation (NE) (eq 2)

$$\sigma_{NMR} = \frac{F^2[C]}{RT}(D_+ + D_-) \tag{2}$$

Room-temperature conductivity measurements calculated by NE exceed those measured with EIS by up to a factor of two, indicating the presence of ion association. However, even very highly ion-associated electrolyte systems tend to show approximately equal cation and anion diffusivities[44] and classical PEO salt complexes always exhibit $D(Li^+) < D(TFSI^-)$.[37,39] This suggests that the preferential cation transport exhibited in this system with $D(Li^+) > D(TFSI^-)$ is largely due to the presence of water, even for a wide range of Li/water mole ratios. This further supports the claim that the dominant ion transport mechanism is preferential water-assisted vehicular transport, where water occupies most of the solvation shell of Li^+.[42] Conductivity calculated using eq 2 as a function of temperature for the NMR sample set with the least amount of air exposure is shown in Figure S6, with linear regression fitting results listed in Table S3. Unfortunately, the presence of water in the electrolytes prohibits electrochemical transference number measurements with Li electrodes by the Bruce–Vincent method, but the NMR results clearly indicate preferential cation transport.

Furthermore, these water-containing electrolytes do show impressive reductive stability, with cyclic voltammetry of AE1 and AE4 in Figure S7 measuring reductive stabilities of ~1.9 and ~1.5 V versus Li/Li^+, respectively. Figure S8 shows galvanostatic cycling of an LTO/ASPE2/LMO battery configuration over 280 cycles at room temperature. The electrodes used for galvanostatic cycling in these samples were not optimized for use with a solid ASPE, but the data do show in principle lithiation and delithiation with the challenging LTO/LMO electrode couple, which is impossible for the WiSE[6] and even water-in-bisalt electrolytes.[29]

https://dx.doi.org/10.1021/acs.macromol.0c01960
Macromolecules 2021, 54, 2882–2891

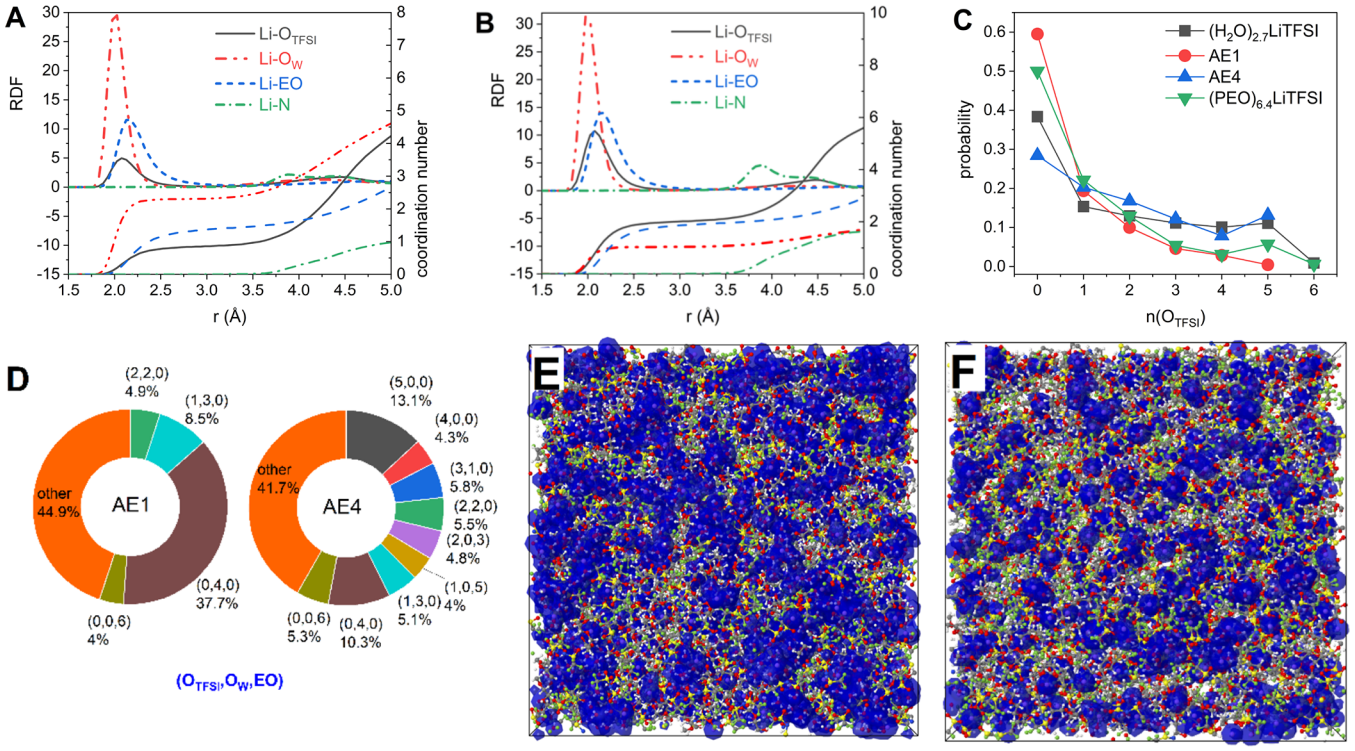

Figure 3. Structural properties from MD simulations: (A, B) radial distribution functions (RDFs) and coordination numbers for Li^+ with oxygen atoms of TFSI, water, and PEO and nitrogen of $TFSI^-$ for AE1 (A) and AE4 (B) electrolytes at 333 K; (C) probability for the Li-$n(O_{TFSI})$, n = 0−6 solvates using the Li−O distance of 2.8 Å; (D) most probable solvates (>4%) for AE1 and AE4 electrolytes with Li coordinated to O_{TFSI}, O_W, and EO within 2.8 Å; and (E, F) $Li^+(H_2O)_n$ domains are highlighted with the blue isosurfaces for AE1 (E) and AE4 (F).

The impressive properties of the pWiSE hybrid electrolytes, along with trends in DSC, EIS, and NMR all pointing to water-assisted vehicular transport as the dominant ion transport mechanism, warranted additional molecular scale insight into the structure and transport mechanism. Molecular dynamics (MD) simulations were performed on liquid AE1 and AE4 pWiSEs and contrasted with the behavior of water-free highly concentrated PEO-LiTFSI (EO/Li = 6.4) and 21 m LiTFSI in the H_2O WiSE. Analysis of the Li^+ cation solvation environment via radial distribution functions (RDFs) is shown in Figure 3A,B, indicating a strong preference for Li^+ to be coordinated by water oxygens (O_W) followed by ether oxygens (EO) of PEO compared to $TFSI^-$ for both AE1 and AE4. This is consistent with a high degree of LiTFSI dissociation in water and to a lesser degree in PEO when sufficient numbers of solvating EO or water are available.[39,45] In the highly concentrated electrolyte AE4, the preference for EO versus O(TFSI) becomes less pronounced because the total number of solvent solvating sites from PEO and water combined drops below 4−5 that are needed to complete the first Li^+ solvation shell; thus, nearly all EO from PEO and water participate in the Li^+ solvation.

Based upon Li−O RDFs, we define the first solvation shell to be 2.8 Å near the location of the first minima. The running coordination numbers shown in Figure 3A,B indicate that the Li^+ cation is primarily coordinated by water (2.3 waters per Li) for AE1 with 1.25 of EO and 0.87 of O($TFSI^-$). When water concentration decreases and salt increases (AE1 → AE4), there is not enough water in AE4 (O_w/Li = 1.177) to complete the Li^+ solvation shell. This leads to a switch from the water-dominated solvation in AE1 to PEO-dominated solvation. At AE4 composition, 93% of all available water and 80% of all EO are bound to Li^+. There is little free solvent in AE4, which helps in extension of electrochemical stability. Due to lack of water and EO for Li^+ solvation as salt concentration increases from AE1 to AE4, the number of O(TFSI) around Li^+ doubles from 0.95 for AE1 to 1.95 for AE4, resulting in a strong contact ion pair (CIP) and aggregate (AGG) formation in AE4. Yet, Figure 3C shows that 58 and 28% of Li^+ do not have any O(TFSI) in its first coordination shell for AE1 and AE4, respectively, indicating that even in these highly concentrated electrolytes, a substantial fraction of the solvent-separated Li^+ cations coexists with Li^+ that is mostly coordinated by 4 or 5 O(TFSI) and resides within the anion network as was previously noted for the WiSE (21 m LiTFSI in H_2O, $(H_2O)_{2.7}$LiTFSI).[42] The LiTFSI salt dissociation ($n(O_{TFSI})$ = 0) decreases in the order of AE1 > PEO-LiTFSI > WiSE > AE4. In these four electrolytes, there is no clear correlation between the number of water or EO and a fraction of free Li^+. However, there seems to be a good correlation between a fraction of free Li^+ and H_2O + 1/2 EO available in our electrolytes, as shown in Figure S9. This correlation suggests that in the solvent-deficient regime that we are exploring, the EO solvating groups are about half as strong/good as water in competing with O(TFSI) and excluding it from the Li^+ first solvation shell. This conclusion is in line with the order of the magnitude of the Li−O(TFSI) RDF first peak being about 1/2 to 1/3 of the magnitude of Li−O_w RDF (see Figure 3A,B).

Further analysis of solvates is shown in Figure 3D. The solvent-separated solvates dominate AE1, with $Li^+(H_2O)_4$ solvation being the most probable followed by $Li^+(EO)(H_2O)_3$ and $Li^+(EO)_2(H_2O)_2$, which is consistent with high fraction (60%) of solvates without any O(TFSI) shown in Figure 3C and is expected to lead to high conductivity. At higher salt

https://dx.doi.org/10.1021/acs.macromol.0c01960
Macromolecules 2021, 54, 2882−2891

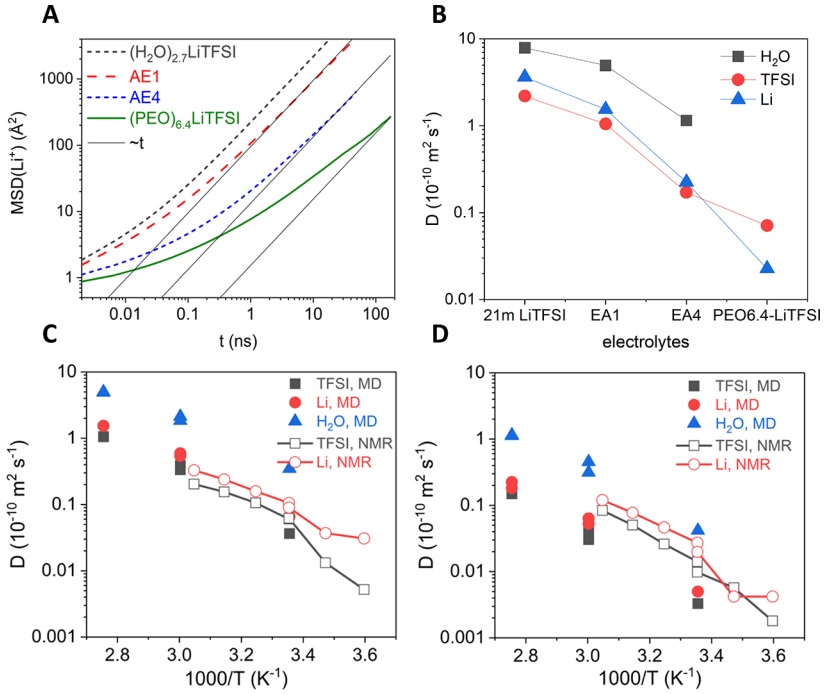

Figure 4. (A) Mean square displacements (MSDs) of the Li^+ cations from MD simulations at 363 K and linear fits indicating where behavior becomes diffusive or linear on the log−log scale; (B) self-diffusion coefficients in 21 m LiTFSI (WiSE), AE1, AE4, and $PEO_{6.4}$-LiTFSI at 363 K from MD simulations (without finite simulation box correction); and (C, D) self-diffusion coefficients of AE1 (C) and AE4 (D) from MD simulations and from pfg-NMR for ASPE1 (C) and ASPE4 (D).

concentration AE4, while the solvent-separated solvates $Li^+(EO)_5$ and $Li^+(H_2O)_4$ are still most probable, their contribution is much smaller and a wide distribution of solvates with Li−O(TFSI) bonds is present (see Figure 3D). The spatial 3D distribution of the water-rich domain is shown in Figure 3E,F. In the AE1 electrolyte, the $Li^+(H_2O)_4$ domain percolates through the whole box, suggesting that sufficient avenues are available for the solvent-separated small $Li^+(H_2O)_4$ to dominate ionic transport over Li^+ transport with and along the PEO segments and by solvent exchange. The $Li^+(H_2O)_4$ domains in AE4 are narrower, more tortuous, and not all interconnected; thus, PEO relaxation is needed to open up these domains and to participate in the Li^+ transport. Moreover, high fraction of the LiTFSI AGG formation in AE4 is expected to contribute to the Li^+ transport through exchange of anions or motion via the charged clusters,[46] which is expected to be less efficient than the $Li^+(H_2O)_4$ transport in the WiSE and AE1.

Changes in hydrogen bonding are examined via analysis of the H_w−O RDFs that show that the position of the first H_w−O_w peak is the same as in pure water (see Figures S10−S12), with the magnitude of the first peak increasing slightly from water to AE1 and AE4. Despite similarity of H_w−O_w RDFs, decreasing water concentration (water > AE1 > AE4) results in a decrease in the number of water hydrogen bonds per water from ∼1 in pure water to 0.4 in AE1 and less than 0.2 for AE4. Thus, the water hydrogen-bond networks become less extended with decreasing water concentration. The hydrogen bonding of water hydrogen to O(TFSI) is similar as the first peaks for H_w−O_w and H_w−O(TFSI) are similar. The second peaks for H_w−EO and H_w−O(TFSI) RDFs are quite different from H_w−O_w because both PEO and $TFSI^-$ are hydrogen-bond acceptors but not donors.[47,48]

Mean square displacements of Li^+ shown in Figure 4A demonstrate that increasing PEO and decreasing water concentration significantly extend the subdiffusive regime from 0.1 ns in the WiSE to 100 ns. In AE1, the Li^+ solvation is dominated by $Li^+(H_2O)_4$ solvates that move through interconnected domains (Figure 3E), and Li^+ motion becomes diffusive rather fast (within 1 ns). In AE4, the Li^+ solvation is dominated by PEO making it more coupled with the polymer dynamics as Li^+ moves with the polymer segment, along the polymer and by switching polymer segments and $TFSI^-$ anions. Analysis of self-diffusion coefficients (see Figure 4B,D) indicates that water diffuses the fastest followed by Li^+ and $TFSI^-$ in both AE1 and AE4 electrolytes, similar to trends observed in the WiSE but opposite from PEO-LiTFSI, where the Li^+ diffusion coefficient is much slower than $TFSI^-$ for the salt-in-polymer regime D(anion) > D(Li). These results corroborate both sets of NMR measurements taken for ASPE1 and ASPE4, which show D(H) > D(Li) > D(F) (Figure 2B and Figures S5 and S6). We attribute an increase in the Li^+ diffusion to the formation of the $Li^+(H_2O)_n$ nanodomain that decouples Li^+ motion from PEO with a significant contribution due to $Li^+(H_2O)_n$ vehicular motion, especially in AE1 where the $Li^+(H_2O)_n$ domains percolate through the simulation box. We find that conductivity calculated from MD simulations for AE1 is in excellent agreement with experiments, while AE4 conductivity in MD simulations is lower than in experiments, as shown in Figure 2A. Part of the difference is due to deficiencies of the force field in this highly concentrated regime, while a small enhancement of conductivity due to limited water uptake during sample transfer is also possible. Nevertheless, the agreement is quite good compared to simulations from other groups for DME/DOL-LiTFSI that predicted slower dynamics by multiple orders of magnitude in the highly concentrated regime.[49]

https://dx.doi.org/10.1021/acs.macromol.0c01960
Macromolecules 2021, 54, 2882−2891

Recent work brought attention to the large discrepancies between t_+ extracted from NMR and impedance measurements with suggestions that t_+(NMR) dramatically overestimates t_+ for highly concentrated electrolytes.[50,51] To compare NMR experimental results with MD simulations, we extracted t^+ following formalism suggested by Wohde et al.[52] based upon Onsager reciprocal relations combined with linear response theory. The full matrix of charge displacements contributing to charge flux (see (eq S4)) is decomposed into the contributions from cation−cation, cation−anion, and anion−anion discussed in the Supporting Information (eqs S1−S5). The transference number under anion blocking conditions (t_+) is defined using two parameters α and β, shown in eqs S5−S7. Unlike the glyme-based solvate ionic liquids where $t_+ < 0.1$ for triglyme (G3)/LiTFSI and tetraglyme (G4)/LiTFSI, we obtain t_+ in the range of 0.4−0.5 for AE1−AE4 from MD simulations. Lower t_+ values of 0.1−0.2 were reported under anion blocking conditions from MD simulations of PEO-LiTFSI at EO/Li = 10 and 6.3.[53] Much higher values are observed for AE1 and AE4 compared to PEO-LiTFSI and glyme-based solvate ionic liquids because of weak anticorrelation parameter β being around −0.4, while G4/LiTFSI solvate ionic liquid exhibited much stronger anticorrelation with $\beta = -0.9$,[51] PEO-LiTFSI showed $\beta = -0.7$.

CONCLUSIONS

We have demonstrated a water-containing solid polymer electrolyte (ASPE) system with high ionic conductivity and preferential cationic transport (D(Li) > D(F)) measured by EIS and NMR compared to D(Li) < D(anion) observed in water-free PEO-LiTFSI and ionic liquids.[39,43,53,54] These exceptional transport properties arise from the disproportionation of the Li^+ solvation environment into mostly water and nonwater solvates as described by MD simulations. The extent to which a network of $Li^+(H_2O)_4$ domains percolate through the system affects the conductivity and the mechanism of Li^+ transport compared to dry PEO-LiTFSI,[39,54] with low-molecular-weight liquid AE1 having a more robust $Li^+(H_2O)_4$ domain network and a higher conductivity than AE4, which has more tortuous $Li^+(H_2O)_4$ domains.

EXPERIMENTAL SECTION

Polymer Electrolyte Preparation. LiTFSI ($LiN(SO_2CF_3)_2$) was purchased from BASF and dissolved in deionized water. Poly(ethylene oxide) (PEO, 10^6 M_v) and poly(ethylene glycol) (PEG, 3350 M_n) were purchased from Sigma-Aldrich. All aqueous solid polymer electrolytes (ASPEs) were fabricated by a solvent-free hot-pressing process shown in Figure S1. PEO, LiTFSI, and deionized water were mixed with a mortar and pestle. The resulting mixture was sealed in a fluoropolymer-lined aluminum pouch and hot-pressed with a Carver press at 85 °C and 1.5 tones to form a thin-film ASPE membrane. Four different compositions were fabricated and characterized, keeping the molar ratio between ethylene oxide (EO) units and LiTFSI the same while changing the amount of water. The compositions of ASPE1−ASPE4 can be found in Table 1. Electrochemical testing was performed using CR2032 coin cells. ASPEs were handled in a normal laboratory atmosphere with care taken to limit the exposure time both during processing and sample making to minimize water content fluctuation. Liquid polymer electrolytes, AE1 and AE4 (the same compositional molar amounts as ASPE1 and ASPE4), were fabricated by mixing low-molecular-weight PEG with LiTFSI and deionized water using a shear mixer. The ASPE is used to designate a high-molecular-weight solid polymer electrolyte, and the AE is used to designate a low-molecular-weight liquid polymer electrolyte for MD simulations.

Differential Scanning Calorimetry. Differential scanning calorimetry (DSC) measurements were conducted on a TA Instruments Q100 DSC. The ASPE samples were sealed in hermetic aluminum pans in an ambient atmosphere shortly after being pressed; the pure PEO samples were sealed in sample pans after drying at 60 °C for 48 h. All samples were measured by a heat/cool/heat method to erase any thermal history in the temperature range from −40 to 100 °C and −100 to 20 °C at a 10 °C/min heating rate and a 10 °C/min cooling rate.

Electrochemical Impedance Spectroscopy. Electrochemical impedance spectroscopy (EIS) for the ASPEs was performed in a stainless steel (SS)/ASPE/SS coin cell setup, with the inclusion of a Teflon spacer to define the thickness and area of the ASPE at 0.025 cm and 0.126 cm^2, respectively. The amount of electrolyte included in a coin cell for impedance spectroscopy was empirically determined such that the volume of the spacer was completely filled with slight excess. The measurements were taken on a Solartron 1287A/1255B platform with a frequency range from 1 MHz to 1 Hz. Measurements were taken in 5 °C decrements from 80 to 0 °C. The cells were annealed for 90 min at each temperature before measurements were taken to ensure thermal equilibrium. Electrolytic conductivities of the liquid polymer electrolytes were determined from impedance scans from 20 Hz to 2 MHz with an amplitude of 20 mV using an Agilent E4980A precision LCR meter. The conductivity cell was made of a Pyrex cell body sealable with a ground glass stopper and calibrated at 0.0954 cm^{-1} for its cell constant at 25 °C. During a measurement, the temperature of the sample cell was ramped down from 80 to 0 °C at 0.1 °C/min in a Tenney Jr. environmental chamber while the impedance was continuously scanned. Conductivities of the sample were then evaluated at the intercepts of the complex impedance curves with the real axis for the corresponding temperatures at which the interceptions occurred.

Pulsed Field Gradient Nuclear Magnetic Resonance. All pulsed field gradient nuclear magnetic resonance (NMR) samples were packed into 5 mm tubes in an ambient atmosphere, and the tubes were then sealed to preserve the same relative humidity value in which they were prepared. NMR experiments were performed by Dr. Steven Greenbaum's group at CUNY at 25 °C with a 300 MHz Varian-S Direct Drive Wide Bore spectrometer equipped with a Doty Scientific PFG probe (DS-1034, 1400 G/cm maximum gradient). Single peaks were observed for ^1H, ^{19}F, and ^7Li resonances centered at 302.7, 280.5, and 117.3 MHz, respectively, corresponding to all hydrogen-, lithium-, and fluorine-containing species, respectively. A PFG-stimulated echo pulse sequence was used. Gradient pulse durations (δ) of 2 to 4 ms and diffusion delays (Δ) of 100 ms were used. The gradient strength (g) was linearly increased with 32 value steps from 1.7 up to 700 G/cm as needed. From each experiment, the integrated intensities (S) as a function of applied gradient (g in T/cm) were obtained. Subsequently, diffusion coefficients (D) were then computed using least-squares fitting of the Stejskal−Tanner equation (where γ is the nuclear gyromagnetic ratio)[55]

$$S = S_0 e^{-D(g\delta\gamma)^2(\Delta-(\delta/3))} \quad (3)$$

Molecular Dynamics Simulation Methodology. Molecular dynamics (MD) simulations were performed for PEO-LiTFSI (EO/Li = 6.4), PEO-LiTFSI-H_2O at two compositions AE1 (H_2O/Li = 3.101; EO/Li = 2.286) and AE4 (H_2O/Li = 1.177; EO/Li = 2.286), and 21 m LiTFSI. PEO chains composed of 64 repeat units. Compositions of the simulation cells are given in Table S4. A many-body polarizable APPLE&P force field was used. The force field parameters for the LiTFSI, PEO-LiTFSI, and LiTFSI-H_2O were taken from previous works.[6,42,53] The functional form of the force field is given elsewhere.[56] The initial configuration for AE1, AE4, and $PEO_{6.4}$-LiTFSI was created by packing solvent and salt in a large box with dimensions of ∼100 to 150 Å and reducing the box size to ∼50 Å over 2−5 ns at 500 K. After that, $PEO_{6.4}$-LiTFSI was equilibrated for 65 ns at 423 K before reducing temperature to 363 K. Equilibration and production runs are shown in Table S5. Two replicas (R1 and

https://dx.doi.org/10.1021/acs.macromol.0c01960
Macromolecules 2021, 54, 2882−2891

R2) with quite different initial solvation environments of Li^+ were simulated for AE1 and AE4.

A multiple timestep integrator was employed with three timesteps: inner, middle, and outer. An inner timestep was set to 0.5 fs for integration of bonded interactions. A middle timestep of 1.5 fs was used for all nonbonded interactions within a truncation distance of 7.0 Å, and an outer timestep of 3.0 fs was used for all nonbonded interactions between 7.0 Å and the nonbonded truncation distances of 12 Å for PEO-LiTFSI, 14 Å for AE1 and AE4, and 16 Å for 21 m LiTFSI. The Ewald summation method was used for the electrostatic interactions between permanent charges with other permanent charges or induced dipole moments with $k = 6^3$ vectors. The reciprocal part of Ewald was calculated every 3.0 fs. Induced dipoles were found self-consistently with convergence criteria of 10^{-9} (electron charge × Å).[2]

■ ASSOCIATED CONTENT

Supporting Information

The Supporting Information is available free of charge at https://pubs.acs.org/doi/10.1021/acs.macromol.0c01960.

Experimental methods and materials, sample preparation, dynamic mechanical analysis, pulsed field gradient nuclear magnetic resonance, electrochemical stability characterization, galvanostatic cycling, and molecular dynamics simulations (PDF)

■ AUTHOR INFORMATION

Corresponding Author

Peter Kofinas − *Department of Chemical and Biomolecular Engineering, University of Maryland, College Park, Maryland 20740, United States;* orcid.org/0000-0001-6657-3037; Email: kofinas@umd.edu

Authors

Matthew D. Widstrom − *Department of Chemical and Biomolecular Engineering, University of Maryland, College Park, Maryland 20740, United States*

Oleg Borodin − *Energy Storage Branch, Sensor and Electron Devices Directorate, Combat Capabilities Development Command U.S. Army Research Laboratory, Adelphi, Maryland 20783, United States;* orcid.org/0000-0002-9428-5291

Kyle B. Ludwig − *Department of Chemical and Biomolecular Engineering, University of Maryland, College Park, Maryland 20740, United States*

Jesse E. Matthews − *Department of Chemical and Biomolecular Engineering, University of Maryland, College Park, Maryland 20740, United States*

Sahana Bhattacharyya − *Department of Physics and Astronomy, Hunter College of the City University of New York, New York 10065, United States*

Mounesha Garaga − *Department of Physics and Astronomy, Hunter College of the City University of New York, New York 10065, United States*

Arthur V. Cresce − *Energy Storage Branch, Sensor and Electron Devices Directorate, Combat Capabilities Development Command U.S. Army Research Laboratory, Adelphi, Maryland 20783, United States*

Angelique Jarry − *Department of Materials Science and Engineering, University of Maryland, College Park, Maryland 20740, United States;* orcid.org/0000-0002-5410-8020

Metecan Erdi − *Department of Chemical and Biomolecular Engineering, University of Maryland, College Park, Maryland 20740, United States*

Chunsheng Wang − *Department of Chemical and Biomolecular Engineering, University of Maryland, College Park, Maryland 20740, United States;* orcid.org/0000-0002-8626-6381

Steven Greenbaum − *Department of Physics and Astronomy, Hunter College of the City University of New York, New York 10065, United States;* orcid.org/0000-0001-5497-5274

Complete contact information is available at: https://pubs.acs.org/10.1021/acs.macromol.0c01960

Notes

The authors declare no competing financial interest.

■ ACKNOWLEDGMENTS

This material is based upon work supported by the National Science Foundation under grant no. CBET2037835 and by the Department of Education grant no. GAANN-P200A180093. The authors would like to thank the U.S. Army Research Laboratory and the Energy Storage Branch for use of their facilities and their continued spirit of governmental and academic collaboration. We thank Aaron Fisher for his previous work that paved the way for this project and the Maryland Nanocenter for their support. All modeling work was supported as part of the Joint Center for Energy Storage Research, an Energy Innovation Hub funded by the U.S. Department of Energy, Office of Science, Basic Energy Sciences through IAA SN2020957 to Army Research Laboratory. The NMR work at the Hunter College was supported in part by the U.S. Office of Naval Research, grant no. N00014-20-1-2186.

■ REFERENCES

(1) Wang, Q.; Jiang, L.; Yu, Y.; Sun, J. Progress of Enhancing the Safety of Lithium Ion Battery from the Electrolyte Aspect. *Nano Energy* **2019**, *55*, 93−114.

(2) Eftekhari, A. High-Energy Aqueous Lithium Batteries. *Adv. Energy Mater.* **2018**, *8*, 1801156.

(3) Forsyth, M.; Porcarelli, L.; Wang, X.; Goujon, N.; Mecerreyes, D. Innovative Electrolytes Based on Ionic Liquids and Polymers for Next-Generation Solid-State Batteries. *Acc. Chem. Res.* **2019**, *52*, 686−694.

(4) Shin, J.-H.; Henderson, W. A.; Passerini, S. Ionic Liquids to the Rescue? Overcoming the Ionic Conductivity Limitations of Polymer Electrolytes. *Electrochem. Commun.* **2003**, *5*, 1016−1020.

(5) Porcarelli, L.; Gerbaldi, C.; Bella, F.; Nair, J. R. Super Soft All-Ethylene Oxide Polymer Electrolyte for Safe All-Solid Lithium Batteries. *Sci. Rep.* **2016**, *6*, 19892.

(6) Suo, L.; Borodin, O.; Gao, T.; Olguin, M.; Ho, J.; Fan, X.; Luo, C.; Wang, C.; Xu, K. "Water-in-Salt" Electrolyte Enables High-Voltage Aqueous Lithium-Ion Chemistries. *Science* **2015**, *350*, 938−943.

(7) Wang, Q.; Sun, J.; Yao, X.; Chen, C. Micro Calorimeter Study on the Thermal Stability of Lithium-Ion Battery Electrolytes. *J. Loss Prev. Process Ind.* **2006**, *19*, 561−569.

(8) Langevin, S. A.; Tan, B.; Freeman, A. W.; Gagnon, J. C.; Hoffman, C. M., Jr.; Logan, M. W.; Maranchi, J. P.; Gerasopoulos, K. UV-Cured Gel Polymer Electrolytes with Improved Stability for Advanced Aqueous Li-Ion Batteries. *Chem. Commun.* **2019**, *55*, 13085−13088.

(9) Edman, L.; Doeff, M. M.; Ferry, A.; Kerr, J.; De Jonghe, L. C. Transport Properties of the Solid Polymer Electrolyte System $P(EO)_nLiTFSI$. *J. Phys. Chem. B* **2000**, *104*, 3476−3480.

(10) Judez, X.; Zhang, H.; Li, C.; González-Marcos, J. A.; Zhou, Z.; Armand, M.; Rodriguez-Martinez, L. M. Lithium Bis(Fluorosulfonyl)-Imide/Poly(Ethylene Oxide) Polymer Electrolyte for All Solid-State Li−S Cell. *J. Phys.Chem. Lett.* **2017**, *8*, 1956−1960.

(11) Rey, I.; Lassègues, J. C.; Grondin, J.; Servant, L. Infrared and Raman Study of the PEO-LiTFSI Polymer Electrolyte. *Electrochim. Acta* **1998**, *43*, 1505−1510.
(12) Murata, K.; Izuchi, S.; Yoshihisa, Y. An Overview of the Research and Development of Solid Polymer Electrolyte Batteries. *Electrochim. Acta* **2000**, *45*, 1501−1508.
(13) Jiang, Y.; Yan, X.; Ma, Z.; Mei, P.; Xiao, W.; You, Q.; Zhang, Y. Development of the PEO Based Solid Polymer Electrolytes for All-Solid State Lithium Ion Batteries. *Polymers* **2018**, *10*, 1237.
(14) Croce, F.; Appetecchi, G. B.; Persi, L.; Scrosati, B. Nanocomposite Polymer Electrolytes for Lithium Batteries. *Nature* **1998**, *394*, 456−458.
(15) Croce, F.; Persi, L.; Scrosati, B.; Serraino-Fiory, F.; Plichta, E.; Hendrickson, M. A. Role of the Ceramic Fillers in Enhancing the Transport Properties of Composite Polymer Electrolytes. *Electrochim. Acta* **2001**, *46*, 2457−2461.
(16) Capiglia, C.; Mustarelli, P.; Quartarone, E.; Tomasi, C.; Magistris, A. Effects of Nanoscale SiO_2 on the Thermal and Transport Properties of Solvent-Free, Poly(Ethylene Oxide) (PEO)-Based Polymer Electrolytes. *Solid State Ionics* **1999**, *118*, 73−79.
(17) Fisher, A. S.; Khalid, M. B.; Kofinas, P. Block Copolymer Electrolyte with Sulfur Based Ionic Liquid for Lithium Batteries. *J. Electrochem. Soc.* **2012**, *159*, A2124−A2129.
(18) Fisher, A. S.; Khalid, M. B.; Widstrom, M.; Kofinas, P. Solid Polymer Electrolytes with Sulfur Based Ionic Liquid for Lithium Batteries. *J. Power Sources* **2011**, *196*, 9767−9773.
(19) Fisher, A. S.; Khalid, M. B.; Widstrom, M.; Kofinas, P. Anion Effects on Solid Polymer Electrolytes Containing Sulfur Based Ionic Liquid for Lithium Batteries. *J. Electrochem. Soc.* **2012**, *159*, A592−A597.
(20) Forsyth, M.; MacFarlane, D. R.; Hill, A. J. Glass Transition and Free Volume Behaviour of Poly(Acrylonitrile)/$LiCF_3SO_3$ Polymer-in-Salt Electrolytes Compared to Poly(Ether Urethane)/$LiClO_4$ Solid Polymer Electrolytes. *Electrochim. Acta* **2000**, *45*, 1243−1247.
(21) Angell, C. A.; Liu, C.; Sanchez, E. Rubbery Solid Electrolytes with Dominant Cationic Transport and High Ambient Conductivity. *Nature* **1993**, *362*, 137−139.
(22) Wang, H.; Wang, Z.; Xue, B.; Meng, Q.; Huang, X.; Chen, L. Polymer-in-Salt like Conduction Behavior of Small-Molecule Electrolytes. *Chem. Commun.* **2004**, *10*, 2186−2187.
(23) Ratner, M. A.; Shriver, D. F. Ion Transport in Solvent-Free Polymers. *Chem. Rev.* **1988**, *88*, 109−124.
(24) Bushkova, O. V.; Popov, S. E.; Yaroslavtseva, T. V.; Zhukovsky, V. M.; Nikiforov, A. E. Ion-Molecular and Ion-Ion Interactions in Solvent-Free Polymer Electrolytes Based on Amorphous Butadiene - Acrylontrile Copolymer and $LiAsF_6$. *Solid State Ionics* **2008**, *178*, 1817−1830.
(25) Ferry, A.; Edman, L.; Forsyth, M.; MacFarlane, D. R.; Sun, J. Connectivity, Ionic Interactions, and Migration in a Fast-Ion-Conducting Polymer-in-Salt Electrolyte Based on Poly(Acrylonitrile) and LiCF3SO3. *J. Appl. Phys.* **1999**, *86*, 2346−2348.
(26) Xu, K.; Wang, C. Batteries: Widening Voltage Windows. *Nat. Energy* **2016**, *1*, 16161.
(27) Suo, L.; Oh, D.; Lin, Y.; Zhuo, Z.; Borodin, O.; Gao, T.; Wang, F.; Kushima, A.; Wang, Z.; Kim, H.-C.; Qi, Y.; Yang, W.; Pan, F.; Li, J.; Xu, K.; Wang, C. How Solid-Electrolyte Interphase Forms in Aqueous Electrolytes. *J. Am. Chem. Soc.* **2017**, *139*, 18670−18680.
(28) Vatamanu, J.; Borodin, O. Ramifications of Water-in-Salt Interfacial Structure at Charged Electrodes for Electrolyte Electrochemical Stability. *J. Phys. Chem. Lett.* **2017**, *8*, 4362−4367.
(29) Suo, L.; Borodin, O.; Sun, W.; Fan, X.; Yang, C.; Wang, F.; Gao, T.; Ma, Z.; Schroeder, M.; von Cresce, A.; Russell, S. M.; Armand, M.; Angell, A.; Xu, K.; Wang, C. Advanced High-Voltage Aqueous Lithium-Ion Battery Enabled by "Water-in-Bisalt" Electrolyte. *Angew. Chem.* **2016**, *128*, 7252−7257.
(30) Yamada, Y.; Usui, K.; Sodeyama, K.; Ko, S.; Tateyama, Y.; Yamada, A. Hydrate-Melt Electrolytes for High-Energy-Density Aqueous Batteries. *Nat. Energy* **2016**, *1*, 16129.
(31) Ko, S.; Yamada, Y.; Miyazaki, K.; Shimada, T.; Watanabe, E.; Tateyama, Y.; Kamiya, T.; Honda, T.; Akikusa, J.; Yamada, A. Lithium-Salt Monohydrate Melt: A Stable Electrolyte for Aqueous Lithium-Ion Batteries. *Electrochem. Commun.* **2019**, *104*, 106488.
(32) Wang, F.; Borodin, O.; Ding, M. S.; Gobet, M.; Vatamanu, J.; Fan, X.; Gao, T.; Eidson, N.; Liang, Y.; Sun, W.; Greenbaum, S.; Xu, K.; Wang, C. Hybrid Aqueous/Non-Aqueous Electrolyte for Safe and High-Energy Li-Ion Batteries. *Joule* **2018**, *2*, 927−937.
(33) Forsyth, M.; Sun, J.; Macfarlane, D. R.; Hill, A. J. Compositional Dependence of Free Volume in PAN/$LiCF_3SO_3$ Polymer-in-Salt Electrolytes and the Effect on Ionic Conductivity. *J. Polym. Sci., Part B: Polym. Phys.* **2000**, *38*, 341−350.
(34) Xie, J.; Liang, Z.; Lu, Y.-C. Molecular Crowding Electrolytes for High-Voltage Aqueous Batteries. *Nat. Mater.* **2020**, *19*, 1006−1011.
(35) Aziz, S. B.; Woo, T. J.; Kadir, M. F. Z.; Ahmed, H. M. A Conceptual Review on Polymer Electrolytes and Ion Transport Models. *J. Sci.: Adv. Mater. Devices* **2018**, *3*, 1−17.
(36) Xu, G. The Effects of Chain Segment Motion on Ionic Diffusion in Solid Polymer Electrolytes. *Solid State Ionics* **1992**, *50*, 345−347.
(37) Gorecki, W.; Jeannin, M.; Belorizky, E.; Roux, C.; Armand, M. Physical Properties of Solid Polymer Electrolyte PEO(LiTFSI) Complexes. *J. Phys.: Condens. Matter* **1995**, *7*, 6823−6832.
(38) Mongcopa, K. I. S.; Tyagi, M.; Mailoa, J. P.; Samsonidze, G.; Kozinsky, B.; Mullin, S. A.; Gribble, D. A.; Watanabe, H.; Balsara, N. P. Relationship between Segmental Dynamics Measured by Quasi-Elastic Neutron Scattering and Conductivity in Polymer Electrolytes. *ACS Macro Lett.* **2018**, *7*, 504−508.
(39) Borodin, O.; Smith, G. D. Mechanism of Ion Transport in Amorphous Poly(Ethylene Oxide)/LiTFSI from Molecular Dynamics Simulations. *Macromolecules* **2006**, *39*, 1620−1629.
(40) Lascaud, S.; Perrier, M.; Vallee, A.; Besner, S.; Prud'homme, J.; Armand, M. Phase Diagrams and Conductivity Behavior of Poly-(Ethylene Oxide)-Molten Salt Rubbery Electrolytes. *Macromolecules* **1994**, *27*, 7469−7477.
(41) Widstrom, M. D.; Ludwig, K. B.; Matthews, J. E.; Jarry, A.; Erdi, M.; Cresce, A. V.; Rubloff, G.; Kofinas, P. Enabling High Performance All-Solid-State Lithium Metal Batteries Using Solid Polymer Electrolytes Plasticized with Ionic Liquid. *Electrochim. Acta* **2020**, *345*, 136156.
(42) Borodin, O.; Suo, L.; Gobet, M.; Ren, X.; Wang, F.; Faraone, A.; Peng, J.; Olguin, M.; Schroeder, M.; Ding, M. S.; Gobrogge, E.; von Wald Cresce, A.; Munoz, S.; Dura, J. A.; Greenbaum, S.; Wang, C.; Xu, K. Liquid Structure with Nano-Heterogeneity Promotes Cationic Transport in Concentrated Electrolytes. *ACS Nano* **2017**, *11*, 10462−10471.
(43) Tsuzuki, S.; Hayamizu, K.; Seki, S. Origin of the Low-Viscosity of [emim][$(FSO_2)_2N$] Ionic Liquid and Its Lithium Salt Mixture: Experimental and Theoretical Study of Self-Diffusion Coefficients, Conductivities, and Intermolecular Interactions. *J. Phys. Chem. B* **2010**, *114*, 16329−16336.
(44) Carbone, L.; Gobet, M.; Peng, J.; Devany, M.; Scrosati, B.; Greenbaum, S.; Hassoun, J. Polyethylene Glycol Dimethyl Ether (PEGDME)-Based Electrolyte for Lithium Metal Battery. *J. Power Sources* **2015**, *299*, 460−464.
(45) MacGlashan, G. S.; Andreev, Y. G.; Bruce, P. G. Structure of the Polymer Electrolyte Poly(Ethylene Oxide)$_6$:$LiAsF_6$. *Nature* **1999**, *398*, 792−794.
(46) Yoon, H.; Best, A. S.; Forsyth, M.; MacFarlane, D. R.; Howlett, P. C. Physical Properties of High Li-Ion Content N-Propyl-N-Methylpyrrolidinium Bis(Fluorosulfonyl)Imide Based Ionic Liquid Electrolytes. *Phys. Chem. Chem. Phys.* **2015**, *17*, 4656−4663.
(47) Smith, G. D.; Bedrov, D.; Borodin, O. Molecular Dynamics Simulation Study of Hydrogen Bonding in Aqueous Poly(Ethylene Oxide) Solutions. *Phys. Rev. Lett.* **2000**, *85*, 5583.
(48) Bedrov, D.; Borodin, O.; Smith, G. D. Molecular Dynamics Simulations of 1,2-Dimethoxyethane/Water Solutions. 1. Conformational and Structural Properties. *J. Phys. Chem. B* **1998**, *102*, 5683−5690.

https://dx.doi.org/10.1021/acs.macromol.0c01960
Macromolecules 2021, 54, 2882−2891

(49) Rajput, N. N.; Murugesan, V.; Shin, Y.; Han, K. S.; Lau, K. C.; Chen, J.; Liu, J.; Curtiss, L. A.; Mueller, K. T.; Persson, K. A. Elucidating the Solvation Structure and Dynamics of Lithium Polysulfides Resulting from Competitive Salt and Solvent Interactions. *Chem. Mater.* **2017**, *29*, 3375−3379.
(50) Dong, D.; Sälzer, F.; Roling, B.; Bedrov, D. How Efficient Is Li^+ Ion Transport in Solvate Ionic Liquids under Anion-Blocking Conditions in a Battery? *Phys. Chem. Chem. Phys.* **2018**, *20*, 29174−29183.
(51) Cho, S.-J.; Yu, D.-E.; Pollard, T. P.; Moon, H.; Jang, M.; Borodin, O.; Lee, S.-Y. Nonflammable Lithium Metal Full Cells with Ultra-High Energy Density Based on Coordinated Carbonate Electrolytes. *iScience* **2020**, *23*, 100844.
(52) Wohde, F.; Balabajew, M.; Roling, B. Li^+ Transference Numbers in Liquid Electrolytes Obtained by Very-Low-Frequency Impedance Spectroscopy at Variable Electrode Distances. *J. Electrochem. Soc.* **2016**, *163*, A714.
(53) Steinrück, H.-G.; Takacs, C. J.; Kim, H.-K.; Mackanic, D. G.; Holladay, B.; Cao, C.; Narayanan, S.; Dufresne, E. M.; Chushkin, Y.; Ruta, B.; Zontone, F.; Will, J.; Borodin, O.; Sinha, S. K.; Srinivasan, V.; Toney, M. F. Concentration and velocity profiles in a polymeric lithium-ion battery electrolyte. *Energy Environ. Sci.* **2020**, *13*, 4312−4321.
(54) Molinari, N.; Mailoa, J. P.; Kozinsky, B. Effect of Salt Concentration on Ion Clustering and Transport in Polymer Solid Electrolytes: A Molecular Dynamics Study of PEO−LiTFSI. *Chem. Mater.* **2018**, *30*, 6298−6306.
(55) Stejskal, E. O.; Tanner, J. E. Spin Diffusion Measurements: Spin Echoes in the Presence of a Time-Dependent Field Gradient. *J. Chem. Phys.* **1965**, *42*, 288−292.
(56) Borodin, O. Polarizable Force Field Development and Molecular Dynamics Simulations of Ionic Liquids. *J. Phys. Chem. B* **2009**, *113*, 11463−11478.

https://dx.doi.org/10.1021/acs.macromol.0c01960
Macromolecules 2021, 54, 2882−2891